Solar Sail resonant periodic orbits in the augmented Earth-Moon Quasi-Bicircular Problem

Marc Jorba-Cuscó
Universitat de Barcelona, Spain, marc@maia.ub.es

Ariadna Farrés
University of Maryland, Baltimore County, United States, ariadna.farresbasiana@nasa.gov

Àngel Jorba
Universitat de Barcelona, Spain, angel@maia.ub.es

Abstract

Solar sailing is a novel way of propelling space probes. It takes advantage of the acceleration produced by photons impacting upon a body, the so-called Solar Radiation Pressure (SRP). Unlike traditional thrusters, the acceleration is continuous and unlimited. We are interested in understanding the dynamics of a spacecraft endowed with a solar sail in the Earth-Moon system. The most commonly used model is a modified version of the Restricted Three Body Problem (RTBP) which includes the effect SRP. Instead, We use the Quasi-Bicircular Problem (QBCP) as a basis model which also includes the gravitation effect of Sun. The resulting model depends on two parameters describing the effectivity and the orientation of the sail. Moreover, the system is a Hamiltonian periodic perturbation of the RTBP. Our goal is to understand how the simplest invariant objects change with respect the sail parameters. We focus on the periodic orbits that replace the Lagrangian equilibrium points as well as the resonant orbits that come from the Lyapunov and Halo families related to the mentioned equilibria.

1 Introduction

The dynamics of the Earth-Moon systems has received increasing interest along the last years. A number of missions that will take place in the vicinity of the Earth and the Moon are being planned. Of special importance is the translunar point i.e. the geometrically defined L_2 Lagrangian point. The mentioned location is flawless for either Moon scientific observation or to establish permanent communication with the Earth from a hypothetical station in the far side of the Moon. To this purpose a special type of trajectories, the Halo orbits [1, 2, 3] have been the classic basis for mission design. This is because a spacecraft following a Halo orbit can, typically, communicate with Earth avoiding the obstruction of Moon's body. There are, nevertheless, other approaches to follow. Solar sailing is among the most promising ones.

The idea behind solar sailing is to endow a spacecraft with a large and highly reflecting surface, the sail. When photons impact upon the sail, some momentum is transferred and the spacecraft receives an acceleration. Despite the variation of velocity due to the sail is much smaller than the ones achieved by a traditional propeller, it is continuous and only limited by the lifespan of the sail. Mathematically, to put a sail in a spacecraft means to modify a classical restricted model by including the effect of Solar Radiation Pressure (SRP), see [4, 5, 6, 7, 8, 9, 10, 11, 12, 13, 14, 15, 16, 17] for works concerning the Earth-Moon system and [18, 19, 20] for the Sun-Earth. SRP modifies the natural dynamics of the model, the invariant structures change their shape, their linear normal behaviour and move around the phase space. Playing with the parameters of the sail, its effectivity and orientation, one can find out different dynamical conditions that can be used for, otherwise inconceivable, mission concepts. For the case of the Earth-Moon system, the most commonly repeated approach is to extend the Earth-Moon Restricted Three Body Problem (RTBP) to include the effect of SRP upon the sail. However, there are several works [21, 22, 23, 24, 25, 26, 27] putting the scientific community on notice of the important effect of Sun's gravity in the Earth-Moon system. The changes on the dynamics, after Sun's gravitational potential addition, are specially important near the translunar and triangular points. Hence, a study involving the translunar point must include Sun's gravity. There is, moreover, another good reason to include Sun's gravity when studding the motion of a solar sail in the Earth-Moon system: it does not increase the dynamical complexity of the model. Indeed, SRP depends

periodically in time, and it does it with the same period as Sun's gravitational potential.

There are several ways to introduce Sun's gravity in the Earth-Moon system but, in seek of simplicity, the most suitable ones are the Bicircular Problem (BCP) and the Quasi-Bicircular Problem (QBCP) (see also a model based in the Hill Problem in [27]). The BCP, the simplest among the two, assumes Earth and Moon to revolve along a circular orbit around their common centre of masses and, at the same time, the Earth-Moon barycentre and Sun to revolve along another circular orbit around the whole system's barycentre. The units and the frame of reference are usually chosen as in the Earth-Moon RTBP so the BCP can be written as a periodic perturbation of the RTBP. Notice that the BCP is not a coherent model i.e. the motion prescribed to the primaries does not follow Newton's laws. Moreover, the BCP is specially weak model for our purposes because it does not count with a dynamical equivalent of the translunar point [21, 28]. The QBCP is a model conceived to be a coherent version of the BCP. Whether the disappearance of the translunar dynamical structure is caused by the non-coherence of the BCP or not, the fact is that this inconvenient is fixed for the QBCP. The QBCP is, therefore, the model for the motion of the primaries we use.

In this work we care about the motion around the libration points L_1 and L_2 of a spacecraft endowed with a solar sail. To do so, we examine how key periodic orbits, with the same period as Sun, change with respect to the parameters of the Sail. These parameters are the effectivity, β, and the pitch angle δ. Summarizing: Section 2 gives a deep explanation on the model we use to undertake this study. The model is obtained by modifying the QBCP to include the effect of SRP upon a perfectly reflecting sail. Section 2 is splitted in two subsections. The first one collects some basic facts about the QBCP and the second one explains how to include the SRP acceleration. Section 3 is devoted to some preliminaries. The aim of this section is to facilitate the reading of the paper pointing out the nature of the orbits we study, the tools and the notation we use. In section 4 we cope with the motion around L_1: We study how nearby orbits change with respect to the parameters of the sail. Section 4 is splitted in two parts: continuation with respect to β and continuation with respect to δ. In these subsections we produce characteristic curves by means of a continuation method that help us to understanding how the dynamics is changed with the parameters. Section 5 is devoted to the study of the dynamics around L_2: We proceed analogously to the case of L_1 and split the section in two parts corresponding to the continuation with respect to β and with respect to δ. Section 6 pays attention on how the SRP helps to reduce (sometimes, dramatically) the large hyperbolicity of some orbits. This stabilization effect make these orbits particularly appealing for mission design as time between station keeping maneuvers can be increased significantly. In Section 7 we point out the effect of Sun's gravity has on the motion of sail dynamics in the Earth-Moon system. Section 8 is devoted to conclusions and further work and Section 9 deals with some specific technical details.

2   The model

The problem of describing the motion of a solar sail in the Earth-Moon system has a natural and unavoidable non-autonomous formulation. Indeed, a suitable model has to take into account the gravitational potential of the Earth and the Moon as well as the position of the Sun. The last is mandatory to describe how Solar Radiation Pressure changes with the motion of the Sun. Without further considerations, a model involving the mentioned properties has to be, at least, periodic in time.

As a first approximation and, in order to keep the model as simple as possible, one uses to consider a modified version of the **Restricted Three Body Problem**. The modification consists in adding to the equations of motion a term corresponding to the SRP. This additional term depends on the position of the Sun and is periodic in time. The influence of Sun's gravity might be added as well. There are two main reasons to do such thing. First, there are several works reporting a remarkable impact due to Sun's gravity in the Earth-Moon system. Second, to add the effect of Sun's gravity (remind that SRP is to be considered) does not increase the **dynamical complexity** of the system. Let us be more precise on what we mean. In an autonomous problem, the simplest invariant objects are equilibrium points, in periodic models, the simplest invariant objects are periodic orbits. As long as one keeps increasing the number of frequencies in the vectorfield, the dimension of the simplest invariant objects keeps increasing. In our case, since SRP is already a perturbation with the same period as the Sun, it does not matter if Sun's gravity is included or not, the simplest invariant objects are periodic orbits with the same period as the Sun.

2.1   The Quasi-Bicircular Problem

The Quasi-Bicircular Problem (QBCP) is a restricted version of the Four Body problem. The model, introduced by C. Simó, is a coherent version of the Bicircular Problem. To construct the model, one prescribes a motion to the primaries which is a solution of the general Three Body Problem for the Earth-Moon-Sun parameters. The strategy is to look for a solution that, at the initial time, the three masses are aligned and impose them to repeat this configuration after a synodical month. We refer to [21] for a deep explanation of the procedure. Also to [29, 30] where the Sun-Jupiter-Saturn case is considered. With respect to the cited works, we point out that the corresponding authors follow different strategies to find this particular solution of the Three Body Problem. In [21] the authors build a specific algebraic manipulator to find directly the Fourier coefficients (up to a certain order). In [29] the approach is to use a continuation method to go from an easy to compute solution of the Two Body Problem to the desired one by moving the mass of Saturn.

The quasi-bicircular solution of the Earth-Moon-Sun system is planar i.e. the three bodies move in the same plane. After the quasi-bicircular solution is computed one can write the equations of motion of the test particle, prescribing the quasi-bicircular solution as motion for the primaries. It is usual to compute the

quasi-bicircular solution in the Jacobi frame, however, if one has the purpose of describing the dynamics in the Earth-Moon vicinity, it is suitable to use the frame of reference corresponding to the Earth-Moon RTBP. To do so, one has to perform three different transformations. First, one has to use a translation to move the origin from the global barycentre to the Earth and Moon centre of masses. Second, one has to use a rotating (synodic) frame to keep the Earth and the Moon fixed on the horizontal axis. Third, the unit of length is scaled so the distance between the Earth and the Moon is equal to one. The units of mass and time which are usually selected in the Earth-Moon RTBP can be imposed already in the Jacobi formulation of the Three Body Problem.

The resulting model is a Hamiltonian system with three and a half degrees of freedom. The Hamiltonian function can be written as

$$
\begin{aligned}
H = {} & \frac{1}{2}\alpha_1(p_x^2 + p_y^2 + p_z^2) + \alpha_2(p_x x + p_y y + p_z z) \\
& + \alpha_3(p_x y - p_y x) + \alpha_4 x + \alpha_5 y \\
& - \alpha_6\left(\frac{1-\mu}{r_{pe}} + \frac{\mu}{r_{pm}} + \frac{m_S}{r_{ps}}\right),
\end{aligned} \quad (1)
$$

where, $r_{pe}^2 = (x-\mu)^2 + y^2 + z^2$, $r_{pm}^2 = (x-\mu+1)^2 + y^2 + z^2$, $r_{ps}^2 = (x-\alpha_7)^2 + (y-\alpha_8)^2 + z^2$, and for $i = 1, \ldots, 8$ α_i is a real-valued periodic function. That is,

$$
\alpha_i(\theta) = a_0^i + \sum_{k \geq 0} a_k^i \cos k\theta + \sum_{k \geq 0} b_k^i \sin k\theta.
$$

Here, $\theta = \omega_S t$ and ω_S is the frequency of Sun. We name T_S the period of Sun. It holds $T_S = 2\pi/\omega_S$. The periodic function α_i is odd for $i = 1, 3, 4, 6, 7$ and even for $i = 2, 5, 8$. Obviously one can only have a numerical approximation of these functions. In this case, we take advantage on the computations done in [21] and take the same values for the Fourier coefficients of the periodic functions α_i's. These periodic functions are the manifestation of several features of the model. Concretely,

(i) $(\alpha_7, \alpha_8, 0)$ is the position of Sun in the plane of motion of the primaries.

(ii) α_1, α_2, α_3 and α_6 capture the fact that the distance between Earth and Moon is not constant.

(iii) α_4 and α_5 take into account the Coriolis effect due to the rotating frame of reference.

It is easy to see that the Hamiltonian function (1) has the symmetry $(\theta, x, y, z, \dot{x}, \dot{y}, \dot{z}) \mapsto (-\theta, x, -y, z, -\dot{x}, \dot{y}, -\dot{z})$, $\dot{x} = p_x + y$, $\dot{y} = p_y - x$, $\dot{z} = p_z$.

2.2 Modeling SRP

The Solar Radiation Pressure (SRP) is the pressure exerted by the impact of photons upon a body. While the incidence of this effect is negligible in our everyday experience, SRP has a remarkable impact in the Solar System and some phenomena cannot be explained without it. Perhaps two of the most relevant ones are the existence of comet tails and the motion of interstellar dust. In both cases SRP acts together with the solar wind. The idea behind solar sailing is to take advantage on this effect to move a spacecraft. The concept of this type of thrust is radically different from the traditional ones, hence solar sails have to be used in different contexts. The main advantage of solar sailing is that the propellant is unlimited (the only limitation is the lifespan of the sail). The main inconvenient is that the acceleration given by SRP is much smaller than the one achieved by a traditional thruster. The force exerted by SRP can be derived from any theory consistent with the fact that light (as a particle) can push matter. In [31] the author describes how the action of SRP is derived from both quantum mechanics and electromagnetic point of view. It holds that, as a first approximation, the pressure on some point at distance r to the Sun is given by

$$
\mathcal{P} = \frac{W_E}{c}\left(\frac{R_E}{r}\right)^2, \qquad W_E = \frac{L_S}{4\pi R_E^2}.
$$

where, R_E is the Earth-Sun distance, L_S is the solar luminosity and c is the speed of light. Notice that this is an inverse square law, fact that eases to compare SRP and Solar gravitation. This law considers the Sun as a punctual mass, if one takes into account the angular size of the solar disk, the expression for $\mathcal{P}$ becomes more sophisticated [31]. We stress that, if the photons impact on a perfectly reflecting surface, the observed pressure is twice this value of $\mathcal{P}$ (due to the action-reaction law). Consider now a solar sail with area A and mass m. Suppose also that the sail is **perfectly reflecting**. The force exerted upon the spacecraft by SRP is given by

$$
F_{SS} = 2\mathcal{P}A\langle \vec{r}, \vec{n}\rangle^2 \vec{n},
$$

where $\vec{r}$ is the Sun-sail vector and $\vec{n}$ a the unitary normal vector to the surface of the sail. As we already have pointed out, the solar sail acceleration can be written in terms of Sun's gravitational acceleration

$$
\vec{a}_{SS} = \beta \frac{Gm_s}{r_{PS}^2}\langle \vec{r}, \vec{n}\rangle^2 \vec{n}, \quad (2)
$$

where m_S is the mass of the Sun, G is the universal gravitational constant and β is the so-called lightness number of the Sail. The lightness number is the ratio between SRP and Sun's gravitational acceleration. It is used to quantify the effectivity of the sail. Real solar sails in space have achieved the following values: $\beta = 0.001$ (IKAROS), $\beta = 0.08$ (Nanosail) and $\beta = 0.011$ (LightSail-1). When $\beta = 1$ the magnitude of SRP acceleration (if the sail is perpendicular to the Sun) is the same as Sun's gravitational acceleration but with opposite direction. Indeed,

$$
\beta = \frac{\sigma^*}{\sigma}, \qquad \sigma^* = \frac{L_E}{2\pi Gm_S c} \approx 1.53 g/m^2.
$$

The quotient $\sigma = m/A$ is the sail loading parameter and parametrizes the performance of the Sail. In Table 1, a numerical relation between the lightness number, the loading parameter, the characteristic acceleration and the area of a sail with fixed mass is provided.

Table 1: Relation between β, the sail lightness number, σ the inverse of the area-to-mass ratio of the satellite, a_0, the characteristic acceleration and A, the sail area requirements for 10 kg of total mass [32].

β	σ (g/m^2)	a_0 (mm/s^2)	Area (m^2)
0.01	153.0	0.059935	$\approx 8 \times 8$
0.02	76.5	0.119869	$\approx 12 \times 12$
0.03	51.0	0.179804	$\approx 14 \times 14$
0.04	38.25	0.239739	$\approx 16 \times 16$
0.05	30.6	0.359608	$\approx 20 \times 20$

Let us take a look again to expression (2). The term Gm_S/r_{PS}^2, depends on the position of the sail in the Earth-Moon system. However, this dependence is negligible compared to the dependence on the position of Sun. Hence, it is usual [9, 33, 14, 13, 15] to perform the following simplification:

$$\frac{m_S}{r_{PS}^2} \approx \frac{m_S}{x_S^2 + y_S^2}.$$

Here, the vector $(x_S, y_S, 0)$ stands the position of Sun in the plane of motion of the primaries. Therefore, it is assumed that, in terms of the characteristic acceleration, the sail can be regarded as frozen at the centre of masses of the Earth-Moon system.

Now we can adjust the SRP acceleration to the features of the QBCP. In the first place, the characteristic acceleration is modified to take into account the non-constant distance between Earth and Moon, that is,

$$\alpha_6 \frac{m_S}{\alpha_7^2 + \alpha_8^2} = \alpha_6 \frac{m_S}{D^2},$$

where $D^2 = \alpha_7^2 + \alpha_8^2$. We only have to determine the orientation of the sail. The unitary vector $\vec{r}$ is taken as the unitary Sun-Earth-Moon barycentre direction, that is

$$\vec{r} = (\tilde{\alpha}_7, \tilde{\alpha}_8, 0) = \frac{(\alpha_7, \alpha_8, 0)}{D}$$

Let us choose $\vec{\gamma}$ orthogonal to $\vec{r}$ i.e. $\vec{\gamma} = (-\tilde{\alpha}_8, \tilde{\alpha}_7, 0)$. Finally, $\vec{n} = \mathcal{R}_\delta^{\vec{\gamma}} \vec{r}$, where $\mathcal{R}_\delta^{\vec{\gamma}}$ stands for the rotation matrix of angle δ along $\vec{\gamma}$ i. e. $\vec{n} =$

$$\begin{pmatrix} c\,\delta + \tilde{\alpha}_8^2(1 - c\,\delta) & -\tilde{\alpha}_8\tilde{\alpha}_7(1 - c\,\delta) & \tilde{\alpha}_7\,s\,\delta \\ -\tilde{\alpha}_8\tilde{\alpha}_7(1 - c\,\delta) & c\,\delta + \tilde{\alpha}_7^2(1 - c\,\delta) & -\tilde{\alpha}_8\,s\,\delta \\ -\tilde{\alpha}_7\,s\,\delta & -\tilde{\alpha}_8\,s\,\delta & c\,\delta \end{pmatrix} \cdot \begin{pmatrix} \tilde{\alpha}_7 \\ \tilde{\alpha}_8 \\ 0 \end{pmatrix}$$
$$= \begin{pmatrix} \tilde{\alpha}_7\,c\,\delta \\ \tilde{\alpha}_8\,c\,\delta \\ s\,\delta \end{pmatrix}.$$

To avoid heavy notation, we use $c\,\delta$ to indicate $\cos\delta$ and $s\,\delta$ to denote $\sin\delta$.

Now, taking into account that, by construction, the angle between $\vec{r}$ and $\vec{n}$ is δ, $\langle\vec{r}, \vec{n}\rangle = \cos\delta$, the acceleration due to SRP

is

$$\vec{a}_{SS} = \alpha_6 \beta \frac{m_S}{D^2} \cos^2\delta \begin{pmatrix} \tilde{\alpha}_7 \cos\delta \\ \tilde{\alpha}_8 \cos\delta \\ \sin\delta \end{pmatrix}.$$

The resulting model is a three and a half degrees of freedom Hamiltonian system whose dynamics is given by the following function:

$$\begin{aligned} H = &\frac{1}{2}\alpha_1(p_x^2 + p_y^2 + p_z^2) + \alpha_2(p_x x + p_y y + p_z z) \\ &+ \alpha_3(p_x y - p_y x) + \alpha_4 x + \alpha_5 y \\ &- \alpha_6\left(\frac{1 - \mu}{r_{pe}} + \frac{\mu}{r_{pm}} + \frac{m_S}{r_{ps}}\right) - \frac{\beta m_S}{a_S^2}\langle\vec{ss}, \vec{e}\rangle. \end{aligned}$$

$$(3)$$

Here, the vector $\vec{ss}$ is given, component by component, as:

$$\begin{aligned} ss^x &= \cos^3\delta\,\tilde{\alpha}_7, \\ ss^y &= \cos^3\delta\,\tilde{\alpha}_8, \\ ss^z &= \cos^2\delta\sin\delta, \end{aligned}$$

and $\vec{e} = (x, y, z)^T$. It is easy to see that the Hamiltonian function (3) has the symmetry

$$(\theta, x, y, z, \dot{x}, \dot{y}, \dot{z}, \beta, \delta) \mapsto (-\theta, x, y, -z, \dot{x}, \dot{y}, -\dot{z}, \beta, -\delta), \quad (4)$$

$$\dot{x} = p_x + y, \quad \dot{y} = p_y - x, \quad \dot{z} = p_z.$$

On the orientation of the sail: The parameter δ (the pitch angle) defines the orientation of the sail in space. The angle δ provides out-of-plane acceleration if $\delta \neq 0$. In the case when $\delta = 0$ there is no out-of-plane acceleration. Therefore, the orbits that are confined in the plane of the primaries stay confined when the sail is added. To study these confined motion one can dispense with the vertical motion and the system can be considered a two and a half degrees of freedom Hamiltonian system. It is easy to see that, for a fixed value of β, the magnitude of SRP acceleration is maximized at $\delta = 0$, while the maximum out-of-plane acceleration is given by $\pm\delta_{max} = \pm\sin^{-1}(1/\sqrt{3})$. The pitch angle has physical sense when $\delta \in [-\pi/2, \pi/2]$. If one of the pitch angle is set to $\pi/2$ or $-\pi/2$, SRP vanishes.

3 Preliminaries: The Resonant orbits of the QBCP

Let us set our mind in the context of the RTBP and remind that, as application of the Lyapunov centre theorem, we know that a family of periodic orbits (which can be parametrized by the period) grow along each elliptic direction related to each Lagrangian equilibrium point. Both, L_1 and L_2 have two of these elliptic directions.

When the perturbation due to the gravity of Sun is considered, almost all (in the measure theory sense) these periodic orbits are replaced by two-dimensional invariant tori. Essentially, the periodic orbits gain the frequency of Sun. Anyhow, there is a group of these periodic orbits that remains being periodic when Sun's

gravitational potential is considered. These orbits are the ones whose period is a (rational) multiple of the period of Sun. These orbits are called **resonant orbits**.

Summarizing, there is a set of periodic orbits of the RTBP, close to the Lagrangian points L_1 and L_2, that can be continued as a T_S-periodic orbits to the QBCP. These computations can be found in [21]. In this work the authors set labels for the orbits depending on the Lagrangian points which they are related to and their properties. When these orbits are continued from the RTBP to the QBCP several bifurcation points appear. That is, it is usual that a resonant orbit of the RTBP has several related orbits in the QBCP. The orbits of the QBCP are labeled taking into account these relations.

In Table 2 we summarize the given information. The orbits are labeled according to [21]. In the left column we show the label of each resonant orbit of the RTBP. Notice that these labels start with a zero. The first character of each label indicates the libration point the orbit is associated with. The second character refers to the type of family: numbers identify orbits in the Lyapunov family and letters do it for orbits in the Halo family. For instance 12 is a Lyapunov trajectory near to L_1 while $2A^+$ is a Halo orbit related to L_2. The $\pm$ sign as super-index only appears in the Halo orbits. The $+$ stand for trajectories of the Halo family whose initial condition lie above the plane. The sign $-$ denotes the symmetric counterpart below the plane.

In the central columns, we show the order of the resonance and the number of bifurcating orbits appearing during the continuation. Lastly, in the right column, we show the orbits corresponding to the QBCP.

Table 2: Continuation of the low order resonant orbits from the RTBP to the QBCP. The first column contains the label of the orbits corresponding to the RTBP. The second column contains the order of the resonance. The third columns contains number of bifurcating orbits. The fourth column contains the label of the orbits corresponding to the QBCP. See [21] for more details. See text for the color code.

RTBP	RES	BIF	QBCP
012	$1:2$	2	12, 13
014	$1:1$	4	14, 15, 16, 17
018	$1:1$	4	18, 19, $1A^\pm$, $1B^\pm$
01C	$1:3$	2	$1C^\pm$, $1D^\pm$, $1N^\pm$
01E	$1:3$	2	$1E^\pm$, $1F^\pm$
022	$1:2$	4	22, 23, 24, 25
026	$1:6$	4	26, 27, 28, 29
02A	$1:2$	4	$2A^\pm$, $2B^\pm$, $2C^\pm$, $2D^\pm$
02E	$1:3$	2	$2E^\pm$, $2F^\pm$
026	$1:4$	2	$2G^\pm$, $2H^\pm$

On the color code: We have added a color code to indicate the linear normal behaviour of each orbit. Labels in red stand for orbits of type saddle×centre×centre. Labels in green denote

linear character of the kind saddle×saddle×centre. Names in cyan denote totally hyperbolic orbits. The color black denotes totally elliptic orbits. The continuation for the orbits in yellow do not reach the homotopy level of the QBCP and, therefore, are not considered. This color code will be maintained during the whole manuscript. In the plots showing continuation curves, the points are colored according to this pattern. Notice that in other plots such as the ones in which we plot trajectories of the flow, we use different colors and they do not denote any kind of normal behaviour.

Dynamical equivalents of the libration points: The libration points L_1 and L_2 are no longer equilibria in the QBCP. These points are replaced by periodic orbits with the same period as Sun. Usually, in the literature, these orbits are refereed as the **dynamical equivalents** of the Lagrangian points L_1 and L_2. Through this work, we shall referee to these equivalent orbits by the name of the corresponding equilibrium point.

Orbits to be followed: In this work we do not keep track on how all the orbits of Table 2 evolve with respect to the parameters of the sail. We focus on the most relevant ones. Let us give some words on how we choose them. First of all most of the bifurcating orbits end up having trajectories which are close (in the phase space) to each other for any time. From these orbits which are similar, we select just one. On the other hand, there are orbits that are close to collision with one of the primaries (maybe both). These orbits lack of great interest as the effect of SRP is to drive them closer to the primaries but without a substantial change on their shapes. These quasi-colliding orbits are: 14, 15, 16, 17, 18, 19, $1A^\pm$, $1B^\pm$, $1E^\pm$, $1F^\pm$ 26, 27, 28, and 29 . We focus on the orbits L_1, 12, $1C^\pm$, $1N^\pm$, L_2, 22, $2A^\pm$, $2E^\pm$ and $2G^\pm$. The orbits which have not been mentioned are skipped as their trajectories are similar to one of the studied orbits.

The Stroboscopic map: The dynamical system studied in this work is Hamiltonian with three and a half degrees of freedom, that is, the Hamiltonian function has three degrees of freedom and also depends periodically on time. Moreover, all the orbits we keep track on have the same period as the Hamiltonian. A suitable tool to study this kind of systems is the so-called **Stroboscopic map**, i.e. the map obtained from evaluating the flow at the period of the Hamiltonian. As the differential equation is Hamiltonian, the stroboscopic map is symplectic. The periodic orbits with the same period as the vectorfield appear as fixed points of the Stroboscopic. The coordinates of the fixed points represent an initial condition of each orbit in the flow. The stability of the fixed points is given by the differential of the Stroboscopic map and coincides with the monodromy matrix of the corresponding periodic orbit. We shall refer to these invariant object as periodic orbits or fixed points indistinctly.

4   Motion near L_1

In the present section we focus on how the periodic orbits L_1, 12, $1C^{\pm}$ and $1N^{\pm}$ change with respect to the parameters of the sail. We perform a continuation of each of these orbits with respect to the parameter β for a perpendicular sail. Then we move the pitch angle for fixed values of the β.

4.1   Continuation with respect to β

The following set of simulations, fixes the orientation of the sail perpendicular to Sun and continues the periodic orbits L_1, 12, $1C^{\pm}$ and $1N^{\pm}$ with respect to β. Let us check, first, how the dynamical equivalent of L_1 changes. As the sail is perpendicular to Sun, there is no out-of-plane acceleration due to SRP. Therefore, L_1 remains being a planar orbit for all values of β. As the value of β increases, the trace of the orbit becomes larger. Even though the trajectories get bigger in size, the growth with respect to β is slow.

In Figure 1 we show trajectories corresponding to the continuation of L_1 (purple) and 12 (green) with respect to β. The continuation is started at $\beta = 0$ and it is stopped at the value $\beta = 1$. This maximal value of β is chosen in the seek for a clearer picture of the situation. As we mentioned, Figure 1 also shows the dynamical equivalents of 12 for the same values of β. Here the situation is slightly different. First of all, the trajectories grow, becoming larger. Notice that this growth is limited by the presence of the primaries. For some value of β the dynamical equivalents of 12 start to decrease in size and, in fact, until they meet L_1 (at a value of β much larger than what is permitted taking into account the current technology).

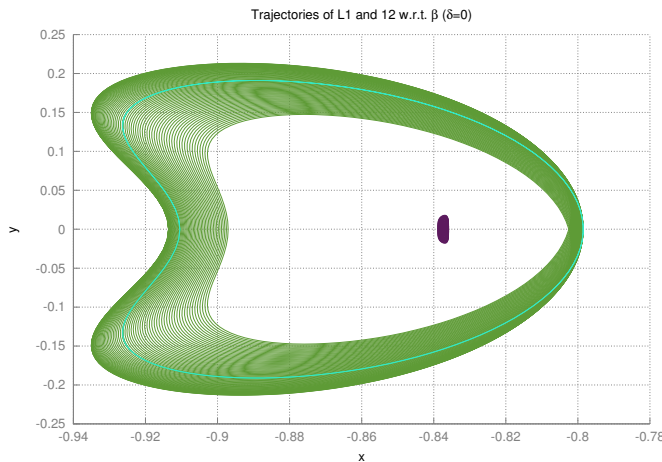We do not show a characteristic curve for this continuation as

Figure 2: Continuations with respect to β of $1C^+$ and $1N^+$ for the fixed values of $\delta = -0.2, -0.5, -1$ and 0. The angles are measured in radians.

in other cases because the interesting phenomena in this continuation occurs for extremely large values of β. It is enough to mention that the periodic orbits L_1 and 12 are connected with respect to β through a saddle-centre bifurcation.

Let us see now how SRP affects the Halo orbit $1C^+$ and $1N^+$ (the situation of $1C^-$ and $1N^-$ is completely symmetric). In Figure 2 it is displayed the continuation of $1C^+$ with respect to β for different values of δ. Notice that, each curve crosses the homotopy level $\{\beta =\}0$ twice: $1C^+$ is the crossing point at the bottom, the one at the top is $1N^+$. The characteristic curves show several bifurcations. At the beginning the curves (red) start with saddle×centre×centre bifurcation. There is a period doubling bifurcation and the curves turn into saddle×saddle×centre. After a transition not seen in Figure 2, due to the scale, the curves switch to centre×complex saddle (magenta). Then the curve turns again into saddle×centre×centre. After a saddle-centre bifurcation the linear character switches finally to saddle×saddle×centre.

4.2   Continuation with respect to δ

Let us study how the fixed point corresponding to the periodic orbit L_1 changes with respect to δ. In Figure 3 we show ten characteristic curves for fixed values of β from $\beta = 0.01$ to $\beta = 0.1$ (with constant step 0.01). The behaviour of all these curves is the same: First, the z value grows for $\delta \in (-\pi/2, -\delta_{max})$. After reaching the homotopy level $\{\delta = -\delta_{max}\}$, the z value starts to decrease, crossing the plane of motion of the primaries. When the continuation curve reaches $\{\delta = \delta_{max}\}$ the z value increases until $\{\delta = \pi/2\}$, where the curve meets again L_1. This is the typical effect of SRP on the trajectories when the orientation of the sail changes, at least for small values of β. If we look at the trajectories in the whole phase space, we notice that, for negative values δ, the trajectories are confined above the plane of motion of the primaries, while, for positive values, they

Figure 1: Trajectories corresponding to the continuation of L_1 and 12 with respect to β. The purple trajectories correspond to the dynamical equivalents of L_1 and the green trajectories correspond to the dynamical equivalents of 12. The blue curve denotes the trajectory 12.
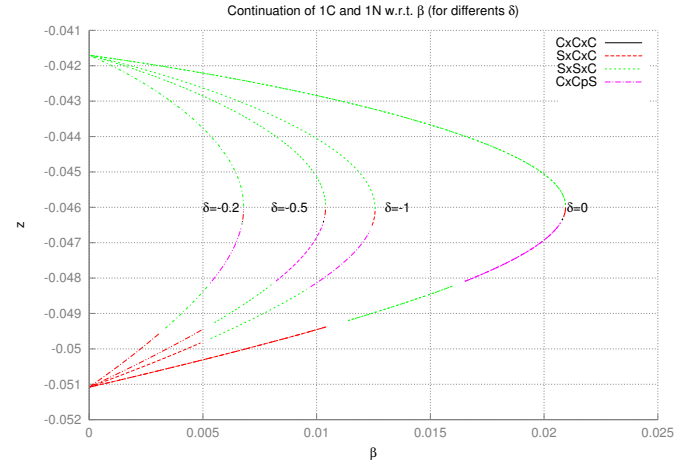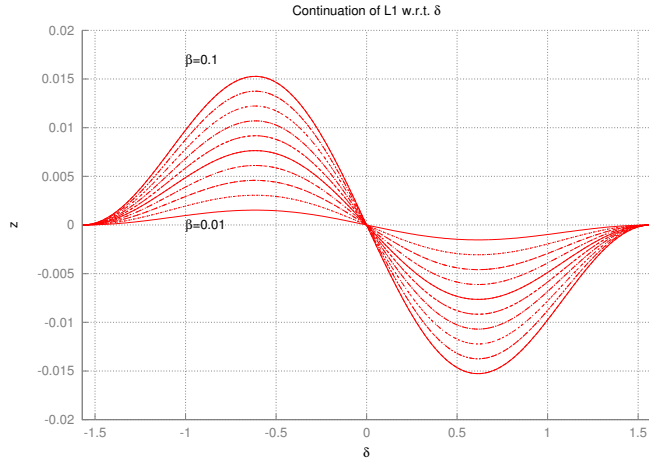
Figure 3: Continuations with respect to δ of L_1. The parameter β is fixed for values between 0.01 and 0.1. The stability type is saddle×centre×centre for all the fixed points.

Figure 5: Trajectories corresponding to the characteristic curve of Figure 4 for $\beta = 0.01$. The blue curve at contained in $\{z = 0\}$ is the trace of orbit associated to $\delta = 0$. The green curve corresponds to the trajectory with $\delta = -\delta_{max}$. The purple curve to the trajectory with $\delta = \delta_{max}$. See text for more details.

lie below. The linear behaviour is the same for all the values of δ and all the characteristic curves: saddle×centre×centre. The maximal eigenvalue does not change substantially in any of these curves. We remark that the planar orbits near the geometrically defined L_1 are highly unstable, i.e. the maximal eigenvalues have extremely large moduli, in this case, it is of order 10^8 (see Table 3). The effect of SRP on the stability of the orbits is treated in a more deep way in Section 6.

We discuss now the fate of 12 as the parameter δ changes. In Figure 4 we show ten characteristic curves for fixed values of β from $\beta = 0.01$ to $\beta = 0.1$ (with constant step 0.01). The first thing to be said is that the plot shown in Figure 4 can be misleading. We observe that, the fixed point corresponding to 12 is driven below the plane of motion of the primaries for nega-
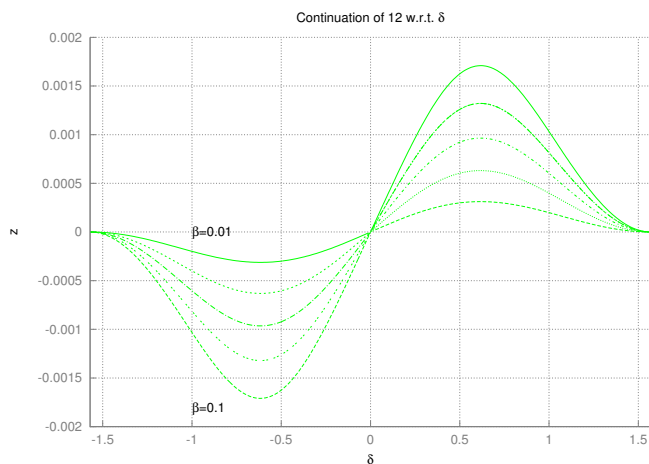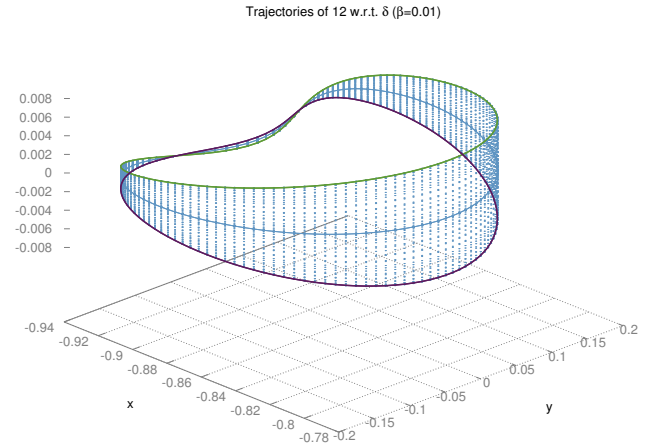

Figure 4: Continuations with respect to δ of 12. The parameter β is fixed for values between 0.01 and 0.1. The stability type is saddle×saddle×centre for all the fixed points.

tive values of δ while one expects the contrary. In Figure 5 we show the trajectories corresponding to the characteristic curve for $\beta = 0.01$. The curve in green is the one with $\delta = -\delta_{max}$, the solid one in blue corresponds to $\delta = 0$ (it is contained in the plane) and the purple one corresponds to $\delta = \delta_{max}$. The blue dashed solid curves are a sample of the curves corresponding to the rest of the initial conditions in the characteristic curve. Notice that, even if the initial condition of the green curve lies below the plane, the trajectory is tilted up. Analogously, the purple curve is tilted down while the initial condition is above the plane. The interesting thing about this behaviour is that, the green and purple curves have a lot of the desirable properties of Halo orbits but lie much closer to the plane. Again, for reasonable values of β the impact of SRP is not strong enough to produce bifurcations. Henceforth, the stability type of all the fixed points of Figure 4 (and the corresponding associated trajectories in Figure 5) is saddle×saddle×centre. Let us analyze the continuation with respect to δ of the Halo orbits $1C^+$ and $1N^+$. The situation of their symmetric counterparts, $1C^-$ and $1N^-$ is completely analogous. For small enough values of β, the effect of the sail's orientation is to move the orbits upwards (for negative values of δ) and downwards (for positive values of δ). Anyhow for $\beta > \beta^* \approx 0.078$ the situation is different. Indeed, if such is the case, the periodic orbits $1C^-$ and $1N^-$ are connected by continuation with respect to the parameter δ. In Figure 6 we display the characteristic curves for $\beta = 0.01, 0.02$ and 0.03 (we only show three curves because to put more does not add relevant information but, due to the superposition of the curves, makes the picture harder to read). One can observe that the curve is splitted in two connected components. The first of these two components is obtained by continuation for negative values of δ (continuation forwards). Indeed, if we start at $1C^+$ and $\delta = -\frac{\pi}{2}$, we find fixed points for some range $\delta \in [-\frac{\pi}{2}, \delta_{tp}^1(\beta)]$, where $\delta_{tp}^1(\beta)$ is a value

of δ, depending on β, for which the curve has a turning point (a saddle-centre bifurcation) and the continuation curve goes back to the homotopy level $\{\delta = -\frac{\pi}{2}\}$. Numerical evidences suggest that $|\delta_{tp}^1|$ is an increasing function of β. The stability type of the orbit changes along the curve. Orbit $1C^+$ is of type saddle $\times$ centre $\times$ centre, while $1N^+$ is of type saddle $\times$ saddle $\times$ centre. There is also a relevant range of δ-values for which the stability type of the curves is complex saddle $\times$ centre. Another stability type appears to fulfill transitions between saddle$\times$centre$\times$centre and complex saddle $\times$ centre (and viceversa): the totally elliptic. However it appears for ranges so small it cannot be observed in Figure 6. The second connected component is obtained by continuing $1C^+$ from $\{\delta = \frac{\pi}{2}\}$ to smaller values of δ (continuation backwards). We obtain new fixed points for $\delta \in \{\delta_{tp}^2(\beta), \frac{\pi}{2}\}$. Again δ_{tp}^2 is a value of δ for which the characteristic curve encounters a turning point. The transition between stability types is similar to the one described for the first component of the curve. The simulations show, as well, that δ_{tp}^2 is an increasing function of β. We would like to notice that both pieces of the curve are, in fact, two different loops (there is a part of each component which does not appear in Figure 6 because they take physically meaningless values of $\delta \notin [-\frac{\pi}{2}, \frac{\pi}{2}]$). The connected component obtained by continuation backwards, the one on the right in Figure 6, is larger, and if β is small enough (as the values we show in Figure 6) it crosses $\{\delta = 0\}$. Notice that there are no fixed points for $\delta \in (\delta_{tp}^1, \delta_{tp}^2)$. The length of this interval increases with β.

A geometrical point of view: To reach a better understanding of the situation described for the continuations of $1C^+$ and $1N^+$ we switch to a more geometrical point of view. As we move the parameters β and δ, we create a surface of fixed points. This surface is compact, with boundary, and embedded in the six-dimensional phase space. It also contains the fixed points $1C^+$ and $1N^+$ corresponding to the QBCP. This surface has a geometric saddle point. In Figure 7 we show several level curves in
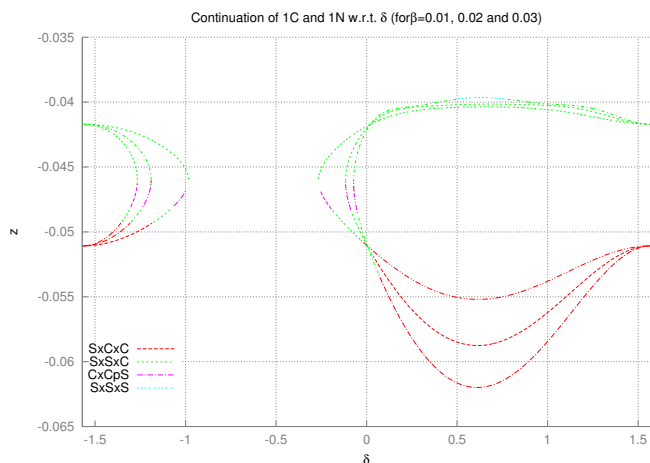

Figure 6: Continuations with respect to δ of $1C^+$ and $1N^+$. The parameter $\beta = 0.01, 0.02$ and 0.03..
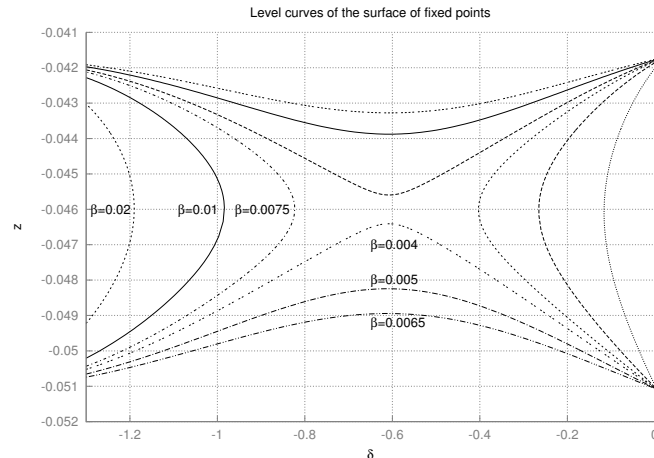

Figure 7: Slices of the surface of fixed points connecting $1C^+$, $1N^+$. In this case, the color do not represent any kind of stability behaviour.

β (continuation curves with respect to δ). Notice that the values of the horizontal axis range between -1.3 and 0. The saddle point is clearly observed.

5 Motion near L_2

In the present section we focus on how the periodic orbits L_2, 22, $2A^\pm$, $2E^\pm$ and $2G^\pm$ change with respect to the parameters of the sail. As in the section devoted to L_1, we first measure the effect of the SRP when the sail is perpendicular to Sun. To do so, we perform a continuation of each of these orbits with respect to the parameter β for a perpendicular sail. Then we move the pitch angle for fixed values of the β.

5.1 Continuation with respect to β

We focus first in the planar orbits. Let us fix $\delta = 0$ and continue L_2 and 22 with respect to β. As we pointed out before, the perpendicularity of the sail keeps these orbits to be planar for all the values of β. Unlike the case of L_1 and 12, the fixed points are not connected by continuation with respect to β (at least, for the values studied in this work). L_2 can be continued, however, to the orbit 24 of Table 2. We recall that orbit 24 bifurcates from 22 when it is continued from the $RTBP$ to the $QBCP$ and that their traces remain close for all time. In practical effects, they can be considered the same orbit. Again, the value of β is too large to be considered to practical purposes (around 4.2). Being realistic on the values of β considered, we can only state that the SRP changes the size and the shape of the periodic orbits L_2. In the case of 22 we have continued it for large values of β seeing small changes in the orbits besides becoming slightly larger. Similarly, the SRP has not a remarkable impact on the halo orbits $2A^\pm$ when the sail is perpendicular to Sun. Not even the size of the orbit is change substantially. We do not provide plots

of these continuations as nothing interesting happens for realistic values of β. The case of the halo orbits $2E^\pm$ and $2G^\pm$ is a not much more interesting. Let us do, however, some comments. First of all, let us notice that these Halo orbits reach much higher values above (below) the plane of motion of the primaries than the orbits $2A^\pm$. Second, they pass much closer to Moon. With these two points under consideration, is to be expected some difference. Indeed, the SRP acts in $2E^\pm$ and $2G^\pm$ displacing the orbits towards the position of Moon and making their traces pass even closer. In fact, with relatively low values of β we can produce colliding trajectories from $2G^\pm$. The linear character o the orbits L_2, 22, $2E^\pm$ and $2G^\pm$ remains unchanged for all the explored values of β when the sail is perpendicular to Sun.

5.2 Continuation with respect to δ

We focus now on the continuation curves obtained by fixing β and changing δ. Let us start with L_2. As in the case of L_1, the effect of SRP to the fixed point L_2 is to move it above the plane (for negative values of δ) and below the plane (for positive values of δ). See Figure 8 for a sample of ten characteristic curves with β ranging from 0.01 to 0.1 with constant step-size. There we see how the fixed points corresponding to L_2 increase its z value, reaching a maximum at $\delta = -\delta_{max}$, then they decrease, crossing the plane at $\delta = 0$, reaching a minimum at $\delta = \delta_{max}$. Finally the fixed points return to the plane of motion of the primaries to meet the QBCP L_2 at the homotopy level $\frac{\pi}{2}$. The stability type of all the curves in Figure 8 is saddle× centre × centre. Let us describe the continuations of 22, $2A^+$ and $2A^-$. Notice that, in this case, $2A^+$ and $2A^-$ are named separately. For sufficiently large values of β, the three orbits are related by continuation and the characteristic curve is splitted in three connected components. We take a look first at Figure 9. This picture is a magnification of Figure 10 and shows the continuation forwards of 22. We show a sample of ten characteristic curves for

Figure 9: Continuation of the orbit 22 and $2A^-$ with respect to δ for fixed values of β. These values of β range between 0.01 and 0.1 with constant step.

which the qualitative behaviour is the same: The method finds fixed points for $\delta \in (-\frac{\pi}{2}, \delta^3_{tp}(\beta))$. Again, $|\delta^3_{tp}|$ increases with β. The turning point corresponds to a saddle-centre bifurcation and the linear behaviour switches from saddle×saddle×centre to saddle×centre×centre. After the turning point, the continuation curve returns back to the homotopy level $\{\delta = \frac{\pi}{2}\}$. Again we see that the initial conditions of 22 move below the plane when we expect to move above and, again, it is a matter of initial conditions. The trajectories are, in fact, tilted up. Moreover, this continuation sets an homotopy from a planar orbit to a Halo one, which makes this particular continuation interesting.

Figure 10 shows the complete picture. The small component on the left are the curves represented in Figure 9. The other small component is the symmetric counterpart: A set of continuation curves (with β between 0.01 an 0.1) connecting 22 with $2A^+$ but by continuation backwards. Let us focus on the long component i.e. the continuation of $2A^+$ forward. These are the ten curves in Figure 10 crossing from the homotopy level $\{\delta = -\frac{\pi}{2}\}$ to the homotopy level $\{\delta = \frac{\pi}{2}\}$. Again, the fixed values of β range from 0.01 to 0.1 with constant step-size. The qualitative behaviour of all these curves is the same. Let us describe it. The characteristic curves start for $\delta = -\frac{\pi}{2}$ at the QBCP $2A^+$. The z coordinate of the fixed points increases its value as $\delta \in (-\frac{\pi}{2}, -\delta_{max})$. For $\delta \in (-\delta_{max}, 0)$, the z value decreases but it is still positive. For $\delta = 0$ the characteristic curves cross the plane and meet a planar orbit. This planar orbit can be obtained also continuing 22 with respect to β when the sail is perpendicular to Sun. Notice that, before the characteristic curve crosses the plane, there is a saddle-centre bifurcation and the stability type changes form saddle×centre×centre to saddle×saddle×centre. After the characteristic curve crosses the plane, the z value keeps decreasing (it encounters another saddle-centre bifurcation) until it reaches the homotopy level $\{\delta = \delta_{max}\}$. These continuations establish homotopies between the orbits $2A^+$ and $2A^-$ i.e. the characteristic curves do not
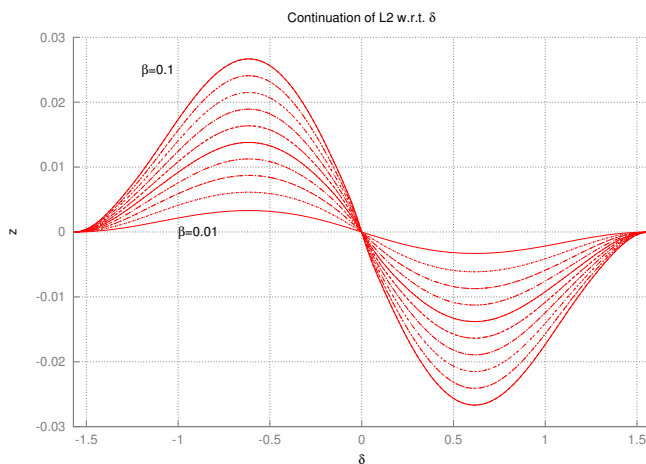

Figure 8: Continuation of the orbit L_2 with respect to δ for fixed values of β. These values of β range between 0.01 and 0.1 with constant step.
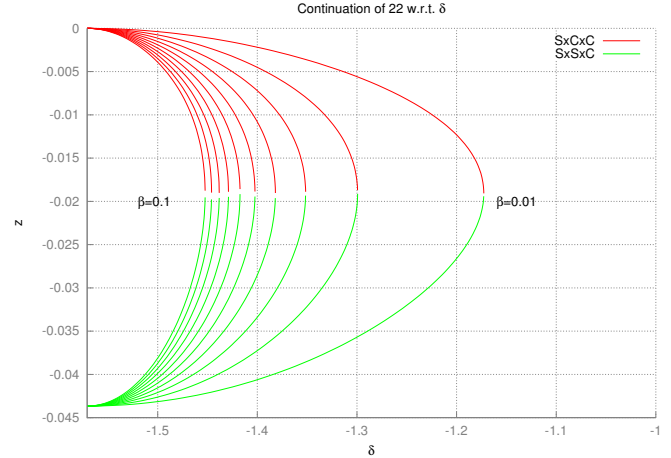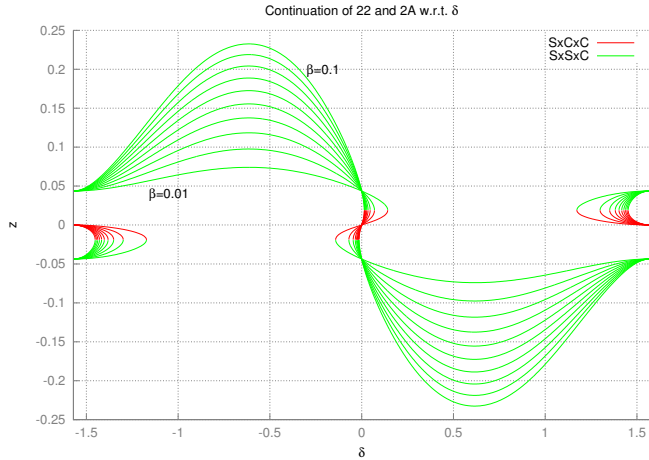
Figure 10: Continuation of the orbit 22, $2A^+$ and $2A^-$ with respect to δ for fixed values of β. These values of β range between 0.01 and 0.1 with constant step.

Figure 11: Continuation of the orbit $2G^+$ with respect to δ for fixed values of β. These values of β range between 0.01 and 0.1 with constant step. The situation for $2G^-$ is analogous.

cross the plane of motion of the primaries again, it ends up at $2A^-$. As in the case of the continuations of $1C^+$ and $1N^+$, there is a geometrical interpretation of the shape of the continuation curves connecting 22, $2A^+$ and $2A^-$. There is a compact with boundary surface of fixed points that contains 22, $2A^+$ and $2A^-$. This surface has also a geometric saddle point at $\{z = 0, \delta = 0\}$. However, in this case, the saddle point is degenerated due to the symmetry of the vectorfield given in (4).

Figure 11 shows the continuation of $2G^+$ (the situation of $2G^-$ is analogous by symmetry) with respect to δ. Again the values of β range from 0.01 to 0.1 with constant step-size. The characteristic curve starts, for $\delta = -\frac{\pi}{2}$, at the QBCP $2G^+$. The z value of the characteristic curve increases for $\delta \in [-\frac{\pi}{2}, -\delta_{max}]$. A number of period doubling-halving processes take place in these curves. We name a period doubling-halving process the mechanism for which a curve of fixed points undergoes a period doubling bifurcation and two families of 2-periodic points branch out and, after, the two branched families join together with the main one. All the changes of the stability type in Figure 11 are produced by this kind of process. Notice that, for $\beta = 0.01$, the characteristic curve only undergo to a single period doubling-halving process near to the homotopy level $\{\delta = \delta_{max}\}$. As β increases, a second process can appear, in Figure 11 it can be observed already for the curve corresponding to $\beta = 0.03$. For sufficiently small values of β we see the repeated pattern for which the z-value reaches its maximum at $\delta = -\delta_{max}$. However as β gets larger, the characteristic curve gets flat near $\delta = -\delta_{max}$. the curve corresponding to $\beta = 0.1$ even displays a local minimum. Notice that, while the z value of the fixed point is actually increasing, the maximal z value of the trajectory is not. This is because the lower part of these orbits is close to Moon and this is an obstacle for the orbits to be moved up. After reaching the plateau around the homotopy level $\{\delta = -\delta_{max}\}$ the characteristic curve decreases its z value until it reaches $\{\delta = \delta_{max}\}$ (passing through a period doubling-halving process). Then, it
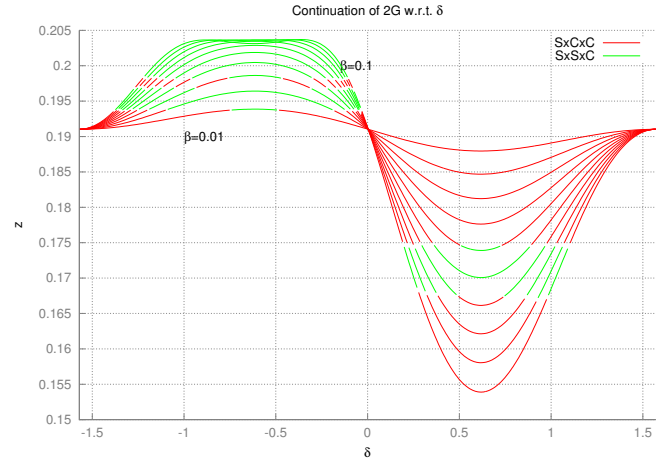
returns back to the original orbit for $\delta = \frac{\pi}{2}$. We show, in Figure 12, the trajectories corresponding to the characteristic curve with $\beta = 0.1$. The solid blue curve corresponds to $\delta = \pm\frac{\pi}{2}$ and it is the trajectory of $2G^+$ in the QBCP. The green trajectory is the one with $\delta = -\delta_{max}$ while the purple curve is the one with $\delta = \delta_{max}$. We observe how the size and the shape of $2G^+$ changes with respect to δ. Notice the difference in size between the green and purple trajectories. The magnitude of the SRP acceleration is the same one for both.

We do not show any continuation with respect to the Halo orbits $2E^\pm$ because it is even more misleading than the ones in Figure 11. Instead of that, we take a look at the trajectories directly. In Figure 13 we show the trajectories corresponding to the con-
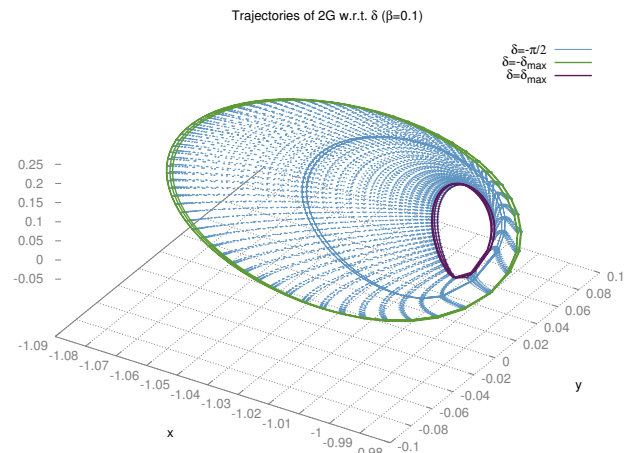

Figure 12: Trajectories corresponding to the characteristic curve with $\beta = 0.1$ of Figure 11. The purple curve corresponds to $\delta = \delta_{max}$ and the green one to $\delta = -\delta_{max}$. See text for more details.
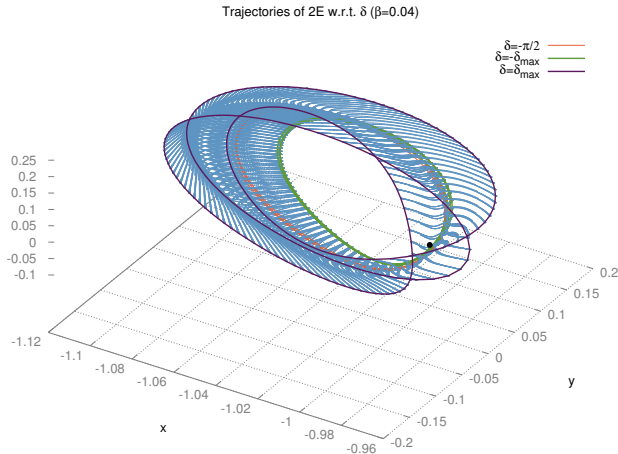
Figure 13: Trajectories corresponding to the continuation of $2E^+$ with respect to δ for $\beta = 0.1$ of Figure 11. The purple curve corresponds to $\delta = \delta_{max}$ and the green one to $\delta = -\delta_{max}$. See text for more details.

tinuation with respect to δ for the fixed value $\beta = 0.04$. The orange trajectory represents $2E^+$, the green trajectory is the one with $\delta = -\delta_{max}$ and the purple curve is the one with $\delta = \delta_{max}$. For all the values of β explored, the continuation takes $2E^+$ to itself. The orbits in this homotopy are large and pass close to the Moon (depicted in Figure 13 as a black point). We do not observe changes in the stability type, it is totally elliptic for all the values of β and δ explored in this work.

6 On the stabilizing effect of SRP

We have been analyzing the different kind of resonant orbits and how they evolve with respect to the parameters of the sail. This study gives insight on potential usage of some of the orbits appearing in it, in view of hypothetical mission design. As almost all these orbits are unstable, the feasibility of such missions relies on station keeping. A reasonable station keeping strategy requires the time span between maneuvers to be as large as possible. High hyperbolicity represents a thread to station keeping. The maximal eigenvalue of the Monodromy matrix (also called maximal Floquet exponent) related to each orbit gives an estimation on how small errors in the initial conditions of the orbits are propagated in a period of Sun. The larger the maximal Floquet exponent is, the more number of maneuvers in one period of Sun (around 29 days) are required to control the probe. The natural motion around the Earth-Moon L_1 and L_2 points is highly unstable. In Table 3 we show the eigenvalues of the periodic orbits replacing L_1 and L_2 (of order 10^8 and 10^6 respectively) in the QBCP. Obviously, it would be mandatory to perform a large number of maneuvers to overcome such instability. Similar values hold for the maximal Floquet exponents of the planar resonant Lyapunov orbits 12 and 22. However, the resonant Halo orbits have much smaller maximal Floquet exponents. These out-of-plane orbits seem, in principle, more appealing as natural

trajectories in which missions could be based on.

Table 3: Eigenvalues of the dynamical equivalents of L_1 and L_2. We only put three for each orbit. The rest are given by their inverses due to the symplectic character of the stroboscopic map.

L_1	(real)	(imag)
1	460182151.57	0
2	-0.987151	0.159784
3	-0.963639	0.267205
L_2	(real)	(imag)
1	2397196.84	0
2	0.995818	0.0913562
3	0.917527	0.3976716

The parameters of the sail establish connections between some of these orbits and, naturally, also does it with the corresponding Floquet exponents. In Figure 14, we display the $\log_{10}$ of the maximal Floquet exponent related to the fixed points of the characteristic curve in Figure 2 (the one with $\delta = 0$). The curve cuts the axis $\{\beta = 0\}$ in two points corresponding to the maximal Floquet exponent of $1C^+$ (the crossing between 1 and 1.5) and the maximal Floquet exponent of $1N^+$ (the crossing point between 2 and 2.5). The curve connects these two values and it reaches the horizontal axis where the maximal Floquet exponent is one. This range of parameters for which the $\log_{10}$ of the maximal Floquet exponent is zero represents, first the transition to complex saddle (totally elliptic points) and also the complex saddle points. Notice that the points with complex saddle linear type are also unstable but they are complex and the modulus is close to 1. We stress the dramatic decay of the maximal Floquet exponent appears for rather large values of β (larger than 0.1), maybe too large for the current technological capabilities. Anyhow, in our opinion, the values are not too large and should be taken into account for future missions: A solar sail permit us to find out-of-plane orbits with small instability. Let us stress that, in Figure 14 the sail is perpendicular to Sun.

To illustrate the effect the orientation of the sail has on the maximal Floquet exponents of orbits near L_2, we take the continuation curve of Figure 10 corresponding to $\beta = 0.1$. This characteristic curve connects $2A^+$ and $2A^-$. Figure 15 shows how the $\log_{10}$ of the maximal Floquet exponent changes with respect to δ. The crossing of the curve with $\{\delta = -\frac{\pi}{2}\}$ is the maximal Floquet exponent of $2A^+$ while the crossing with $\{\delta = \frac{\pi}{2}\}$ corresponds to the maximal Floquet exponent of $2A^-$. By symmetry, the values of these two eigenvalues is the same. What Figure 15 reveals is that being away from the plane gives better stabilization of the sail. For orientation close to $-\delta_{max}$ and δ_{max} the $\log_{10}$ of the maximal Floquet exponent falls blow 4 which means to lose two digits of accuracy less at each period of Sun. On the other hand, the orbits close to the plane are more unstable and the solar sail cannot prevent that. Indeed, at the
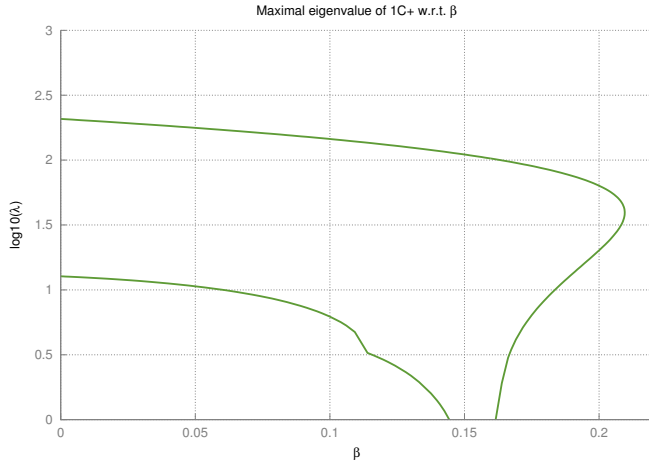
Figure 14: $\log_{10}$ of the maximal eigenvalue of the characteristic curve with $\delta = 0$ appearing in Figure 2.

centre of Figure 15, for δ close to zero, we see how the $\log_{10}$ of the maximal Floquet exponent grows again to values as large as the ones associated to the original orbit and even bigger. Again, the value of β is taken a bit large for the current technology, but it is still suitable to illustrate the stabilizing effect of SRP near L_2.

7   On the effect of Sun's gravity

As we have mentioned, there is a number of works pointing out the important role Sun's gravity plays in the Earth-Moon system [34, 26, 23, 28]. To take into account Sun's gravity in the model, we use one among the simplest ways to introduce Sun's gravity. Besides it is not the first time Sun's gravity is taken into
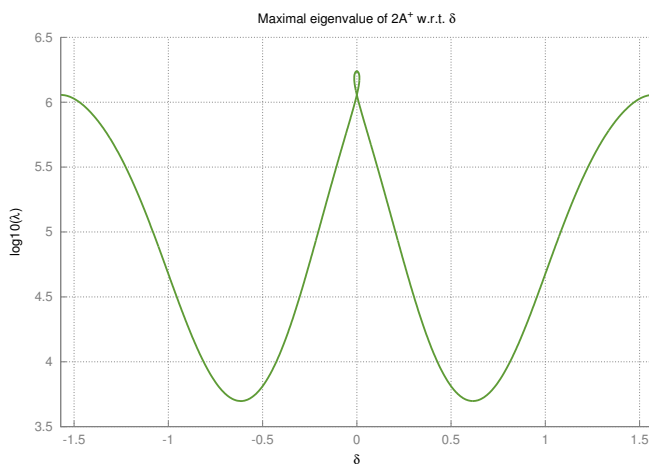
account to study the motion of a solar sail in the Earth-Moon system [15, 33], this is the first work utilizing the QBCP. In the mentioned works, the basis model used is the so called Bicircular Problem (BCP). We refer to [28] for a comparison between models. This comparison reveals that the BCP is not a good option to describe the motion around the translunar point and this vindicates the usage of the QBCP as a basic model for this work. Because in the QBCP the motion of Sun is not circular and the non constant distance between Earth and Moon is taken under consideration substantial disagreements in the gravitational forces acting on a small particle. In Figure 16 we display a comparison between the RTBP and the QBCP. The plot is obtained by taking a grid in the plane of motion of the primaries (the other variables are set to zero) and measuring the normalized differences between vector-fields. The blue points represent the Lagrangian points. The differences are accentuated where the gravity of Earth do not dominate the dynamics. Is specially remarkable the fact that, near Moon and the triangular points, the discrepancy is large. Due to the properties of the QBCP, the acceleration due to SRP upon the sail used in the present work has a small but noticeable disagreement with the solar sail acceleration used in the literature [9, 13, 14, 15]. There, the SRP changes in time according to the assumption that Sun moves in a circular orbit (together with the centre of masses of the Earth-Moon system). It is out of the scope of this paper to provide a comparison between the results of this work and the results obtained if Sun's gravity is not included in the equations of motion. We address the interested reader to [15] where similar simulations (to the ones the present paper shows) are carried out. The disagreement between the two models for the acceleration upon the sail is of order 10^{-3}. This disagreement do not depend on the effectivity of the sail. We point out that the disparity of the results should be taken into account in future studies (according to the goals). The topology of the surfaces of fixed points (near L_1 and L_2) is

Figure 15: $\log_{10}$ of the maximal eigenvalue of the characteristic curve connecting $2A^+$ and $2A^-$ (with $\beta = 0.1$) appearing in Figure 10.
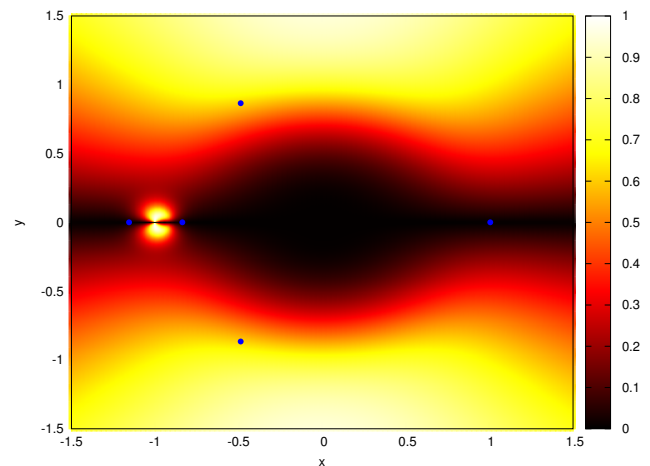

Figure 16: Comparison between the vector-fields of the RTBP and the QBCP. The color code denotes the normalized discrepancy for a grid taken in the plane of motion of the primaries. See text for more details.

severely affected by the way Sun's gravity is introduced.

8   Conclusions and further work

This work studies the motion of a solar sail near the Earth-Moon L_1 and L_2 Lagrangian points. In has been taken under consideration Sun's gravity. A restricted model for the motion of the primaries, the QBCP, is augmented to include the effect of Solar Radiation Pressure. The resulting model is a Hamiltonian of three degrees of freedom and periodic time dependence. The period of the Hamiltonian is the period of Sun. As far as we know, this is the first time in the literature this particular model has been used. We have studied how different periodic orbits (with the same period as Sun) of the QBCP change with respect to the parameters of the sail. Let us stress that, these are the simplest invariant objects of the system. We have used the so-called Stroboscopic map to see these periodic orbits as fixed points. As the sail depends on two parameters, the pitch angle and the effectivity, each of these fixed points has a surface of dynamical equivalents embedded in the phase space. We have studied the geometry and topology of these surfaces by computing sections. These sections are characteristic curves obtained by using the continuation method. We have identified two of these surfaces with special geometric properties. In particular these particular surfaces have a saddle point (one of them is degenerated due to the symmetry of the vectorfield involving the pitch angle). These geometrical properties have a deep impact in the dynamics of the system in terms of existence, linear character and trace of each orbit for a given value of the parameters.

We also report the effect SRP has on the maximal Floquet exponent of some orbits. Among the non-planar resonant Halo orbits we studied in this work, there is a subset of them which can be stabilized i.e. the maximal Floquet exponent can be reduced as much as desired using suitable parameters of the sail. The value of the effectivity required to accomplish that is a little bit larger than the current technological capabilities, around 0.02. The impact of SRP on the large hyperbolicity of the planar orbits is not remarkable. Therefore, these Halo orbits (besides the natural properties that make them interesting) are the ones suitable to be used in mission design as station keeping strategies are reliable. Indeed, the small instability permit to reduce the number of maneuvers to be performed on time.

Finally we give some words on the impact that taking under consideration the gravity of Sun has. We do not provide a deep comparison on the results depending on the inclusion of Sun's gravity but we refer to specific works where similar computations are presented. A short survey of differences spotted is given.

There is certainly much work to be done in this model. This study is a first stage in which we understand how the simplest invariant objects move through the phase space when the parameters are moved. For these orbits we only study the linear behaviour and study of an extended region of the phase space is required. This can be accomplished by using semi-analytical tools or purely numerical ones. For instance, the stable motion can be decoupled from the unstable one by means of the reduction to the centre manifold, which is a semi normal form process. These centre manifold can also be computed numerically which can be better to understand a larger piece of the phase space. Finally, the global aspects of the dynamics can be understood by the computation of large pieces of the unstable manifolds related to these invariant objects. These manifolds can be linearly approximated and numerically grown as usual or approximated to high order by means of the parameterization method.

9   Technical details

The integrations of this work have been carried out using a Taylor method [35] with variable order and step-size. The required accuracy for the integrations has been 10^{-16}. Due to the their highly unstable their character, it has been mandatory to use a multiple shooting approach to compute most of the periodic orbits. A maximum of four sections has been required. All the periodic orbits have been computed with accuracy higher than 10^{-12}. The continuation method we use is the pseudo arclenght method with a Newton scheme as a corrector. The differential of the Stroboscopic (necessary to compute the orbits and study their stability) is obtained by using Jet Transport [36, 37]. All the programs used to perform the computations of this work have been written in C from the scratch. Files containing the values of the parameters used in this work can be found at http://www.maia.ub.edu/~marc/EMQBCP/

References

[1] R.W. Farquhar. *The Control and Use of Libration-point Satellites*. NASA TR R. National Aeronautics and Space Administration, 1970.

[2] R.W. Farquhar and A.A. Kamel. Quasi-periodic orbits about the translunar libration point. *Celestial Mech.*, 7(4):458–473, 1973.

[3] G. Gómez, J.J. Masdemont, and Simó S. Lissajous orbits around halo orbits. *Adv. in the Astronautical Sciences*, 95:117–134, 1997.

[4] C. R. McInnes. Solar sail trajectories at the lunar l2 lagrange point. *Journal of Spacecraft and Rockets*, 30(6):782–784, 1993.

[5] M. T. Ozimek, D. J. Grebow, and K. C. Howell. Design of solar sail trajectories with applications to lunar south pole

coverage. *Journal of Guidance, Control, and Dynamics*, 32(6):1884–1897, 2009.

[6] X. Hou, J. Tang, and L. Liu. On utilization of solar sails in triangular libration point missions in the earth-moon system. *Transactions of the Japan society for aeronautical and space sciences, aerospace technology japan*, 8(ists27):1–5, 2010.

[7] J. Simo and C. R. McInnes. Displaced solar sail orbits: Dynamics and applications. *Advances in the Astronautical Sciences*, 136(2):14–17, 2010.

[8] J. Simo and C. R. McInnes. Designing displaced lunar orbits using low-thrust propulsion. *Journal of Guidance, Control, and Dynamics*, 33(1):259–265, 2010.

[9] J. Simo and C. R. McInnes. Solar sail orbits at the earth-moon libration points. *Communications in Nonlinear Science and Numerical Simulation*, 14(12):4191 – 4196, 2009.

[10] G. Wawrzyniak and K. C. Howell. Generating solar sail trajectories in the earth-moon system using augmented finite-difference methods. *International Journal of Aerospace Engineering*, 2011(Article ID 476197):13 pages, 2011.

[11] G. Wawrzyniak and K. C. Howell. Investigating the design space for solar sail trajectories in the earth-moon system. *The Open Aerospace Engineering Journal*, 4(1):26–44, 2011.

[12] J. Heiligers, S. Hiddink, R. Noomen, and McInnes C. Solar sail periodic orbits in the earth-moon three-body problem. In *Proceedings of the 65th International Astronautical Congress*, Toronto, Canada, 26–30 September 2014.

[13] J. Heiligers, M. Macdonald, and J. S. Parker. Extension of earth-moon libration point orbits with solar sail propulsion. *Astrophysics and Space Science*, 361(7):1–20, 2016.

[14] J. Heiligers, S. Hiddink, R. Noomen, and C. R. McInnes. Solar sail lyapunov and halo orbits in the earth-moon three-body problem. *Acta Astronautica*, 116:25 – 35, 2015.

[15] M. Jorba-Cuscó, A. Farrés, and À. Jorba. Periodic and quasi-periodic motion for a silar sail in the earth-moon system. In *Proceedings of the 67th International Astronautical Congress*, Guadalajara, México, 26–30 September 2016.

[16] R. Sood and K. C. Howell. L4 , l5 solar sail transfers and trajectory design: Solar observations and potential earth trojan exploration. 2016.

[17] J. Heiligers and M. Ceriotti. Orbital dynamics of an oscillating sail in the earth-moon system, 2017.

[18] A. Farrés and À. Jorba. Dynamics of a solar sail near a halo orbit. Preprint, 2010.

[19] A. Farrés and À. Jorba. On the high order approximation of the centre manifold for ODEs. *Discrete Contin. Dyn. Syst. Ser. B*, 14(3):977–1000, 2010.

[20] A. Farrés and À. Jorba. Periodic and quasi-periodic motions of a solar sail close to SL_1 in the Earth-Sun system. *Celestial Mech.*, 107(1-2):233–253, 2010.

[21] M.A. Andreu. *The quasi-bicircular problem*. PhD thesis, Univ. Barcelona, 1998.

[22] M.A. Andreu. Dynamics in the center manifold around L_2 in the quasi-bicircular problem. *Celestial Mech.*, 84(2):105–133, 2002.

[23] E. Castellà and À. Jorba. On the vertical families of two-dimensional tori near the triangular points of the Bicircular problem. *Celestial Mech.*, 76(1):35–54, 2000.

[24] G. Gómez, À. Jorba, J. Masdemont, and C. Simó. A quasiperiodic solution as a substitute of l_4 in the Earth-Moon system. In *Proceedings of the 3rd International Sysmposium on Spacecraft Flight Dynamics*, pages 35–41, ESTEC, Noordwijk, Holand, 1991. ESA Publications Division.

[25] G. Gómez, À. Jorba, J. Masdemont, and C. Simó. Quasiperiodic orbits as a substitute of libration points in the solar system. In A.E. Roy, editor, *Predictability, Stability and Chaos in N-Body Dynamical Systems*, pages 433–438. Plenum Press, 1991.

[26] À. Jorba. A numerical study on the existence of stable motions near the triangular points of the real Earth-Moon system. *Astron. Astrophys.*, 364(1):327–338, 2000.

[27] D. J. Scheeres. The restricted hill four-body problem with applications to the earth–moon–sun system. *Celestial Mechanics and Dynamical Astronomy*, 70(2):75–98, Feb 1998.

[28] M. Jorba-Cuscó, A. Farrés, and Á. Jorba. Two periodic models for the earth-moon system. *Frontiers in Applied Mathematics and Statistics*, 4:32, 2018.

[29] F. Gabern and À. Jorba. A restricted four-body model for the dynamics near the Lagrangian points of the Sun-Jupiter system. *Discrete Contin. Dyn. Syst. Ser. B*, 1(2):143–182, 2001.

[30] F. Gabern. *On the dynamics of the Trojan asteroids*. PhD thesis, Univ. de Barcelona, 2003.

[31] C.R. McInnes. *Solar Sailing: Technology, Dynamics and Mission Applications*. Springer-Praxis, 1999.

[32] B. Dachwald, W. Seboldt, M. Macdonald, G. Mengali, A.A. Quarta, C.R. McInnes, L. Rios-Reyes, D.J. Scheeres, B. Wie, M. Görlich, et al. Potential Solar Sail Degradation Effects on Trajectory and Attitude Control. In *AIAA Guidance, Navigation, and Control Conference and Exhibit*, volume 6172, 2005.

[33] A. Farrés, À. Jorba, and M. Jorba-Cuscó. On the solar sail periodic orbits near the earth-moon libration points. In *Proceedings of the XXIV Congress on differential equations and applications*, Cádiz, Spain, 8–12 June 2015.

[34] V. Companys, G. Gómez, À. Jorba, J. Masdemont, J. Rodríguez, and C. Simó. Use of Earth-Moon libration points for future missions. In K.T. Alfriend, I.M. Ross, A.K. Misra, and C.F. Peters, editors, *AAS/AIAA Astrodynamics Conference*, volume 90 of *Advances in the Astronautical Sciences*, pages 1655–1666, San Diego, U.S.A., 1996. American Astronautical Society.

[35] À. Jorba and M. Zou. A software package for the numerical integration of odes by means of high-order taylor methods. *Experimental Mathematics*, 14(1):99–117, 2005.

[36] A. Farrés, J. Gimeno, Á. Jorba, M. Jorba-Cuscó, N. Miguel, and M. Zou. The parametrization method on Poincaré sections. Preprint, 2018.

[37] D. Pérez-Palau, J. Masdemont, and G. Gómez. Tools to detect structures in dynamical systems using jet transport. *Celestial Mechanics and Dynamical Astronomy*, 123(3):239–262, Nov 2015.